1.6-μm Er:YGG Waveguide Amplifiers

J.I. Mackenzie[a,1], S.V. Kurilchik[a], J.J. Prentice[a], J.A. Grant-Jacob[a], L.G. Carpenter[a], J.C. Gates[a], P.G.R. Smith[a], C.B.E. Gawith[a], H. Riris[b], A.W. Yu[b], R.W. Eason[a]
[a]Optoelectronics Research Centre, University of Southampton, SO17 1BJ, UK
[b]NASA Goddard Space Flight Center, Greenbelt, MD 20771, U.S.A

ABSTRACT

We report on the fabrication and characterization of Er:YGG films suitable for waveguide amplifiers that could in principle be used in integrated path differential absorption lidar systems. Presented is our fabrication technique, comprising pulsed-laser-deposition growth of ~10 μm-thick crystalline films, their channeling via ultraprecision ductile dicing with a diamond-blade, producing optical quality facets and sidewalls, and amplifier performance. Net gain at 1572 nm and 1651 nm is obtained for the first time in Er-doped YGG waveguide amplifiers. Additionally, in a channel waveguide a maximum internal gain of 3.5 dB/cm at the 1533nm peak was realized. Recent crystal film quality improvements promise further performance enhancements needed for the intended application for high-peak power sources in the 1.6-μm spectral region targeting Earth observation systems for monitoring greenhouse gases.

Keywords: Planar waveguide amplifier; Erbium; Pulsed laser deposition; Lidar; Carbon dioxide and methane sensing

1. INTRODUCTION

Understanding the distribution and dynamics of greenhouse gases in the Earth's atmosphere is one of the priorities highlighted in the latest decadal survey for Earth observation from space [1]. To achieve this, Integrated Path Differential Absorption (IPDA) lidar from earth-orbiting satellites is being pursued as a tool to map various gaseous species in our atmosphere. Sources in the 1.6-μm regime are well suited for characterizing two key greenhouse gases, carbon dioxide (CO_2) and methane (CH_4), as there are significant absorption features and efficient photodetectors in this spectral band. A clear challenge for operating in this spectral regime is achieving sufficient pulse energy at the relevant wavelengths of interest and linewidths. In the case of CH_4 a prominent absorption feature is at 1651 nm, around the center of the telecommunications U-band, while for CO_2 the optimal absorption is in the L-band at 1572 nm. Erbium-doped fiber amplifiers cannot reach the required peak-power and linewidth characteristics needed for airborne campaigns, limited by the onset of Stimulated Brillouin Scattering (SBS), and as such alternate amplifier architectures are being explored. Planar Waveguide Amplifiers (PWAs) are one option for realizing sufficient gain in compact devices that may enable mJ-class pulse energies to be achieved.

Yttrium Gadolinium Garnet (YGG) has been identified as an active medium with emission lines matching absorption features for greenhouse gases [2, 3]. As a crystalline host with better power-handling capabilities than glass, and higher gains at the longer wavelengths of interest, relatively short device lengths can be exploited, which helps to raise the SBS threshold that would otherwise degrade the narrow-band seed characteristics. Therefore, Master Oscillator Power Amplifier (MOPA) configurations based upon low-loss PWAs offer a potential solution for direct amplification of low-power single-frequency diode-lasers up to the power levels required for IPDA lidar. A PWA system has already been demonstrated in an airborne campaign, with ytterbium-doped Yttrium Aluminum Garnet (Yb:YAG) as the gain medium [4], proving that it is a viable source architecture for future observation systems.

In this paper we present the latest developments in the fabrication of low-loss planar waveguides comprising Er-doped YGG via pulsed laser deposition (PLD), expanding on our previous work [5]. A further process step, involving precision dicing in the ductile regime, was then used to produce ridge channel waveguides, with optical quality side- and end-facets. We report on the characterization of these waveguides and gain measurements at the key wavelengths for IPDA lidar. These active waveguides are promising candidates for amplifiers in the spectral regions of interest.

[1] J.I.Mackenzie@soton.ac.uk; phone +442380592693; www.orc.soton.ac.uk

2. METHODOLOGY

2.1 Pulsed Laser Deposition

PLD is a mature physical vapor deposition technique and a detailed description of the setup we have used can be found in [6]. To briefly describe the process however, PLD starts with a high-energy pulsed UV laser being focused onto a target in a controlled low-pressure background-gas environment and the resulting plasma-plume propagates across the chamber and is deposited onto a heated substrate, as shown in Fig 1. The desired crystal film growth occurs when the substrate temperature is a significant fraction of the growing crystal's melting point. Employing ceramic targets, which have lower ablation thresholds than single crystals, it is possible to tailor the composition to control the grown crystal's stoichiometry [7]. In this way, we have studied the growth of a wide range of oxides, including garnets [7] and sesquioxides [8], with the intent of engineering the refractive-index profile and the spectroscopic properties on the sub-micron level.

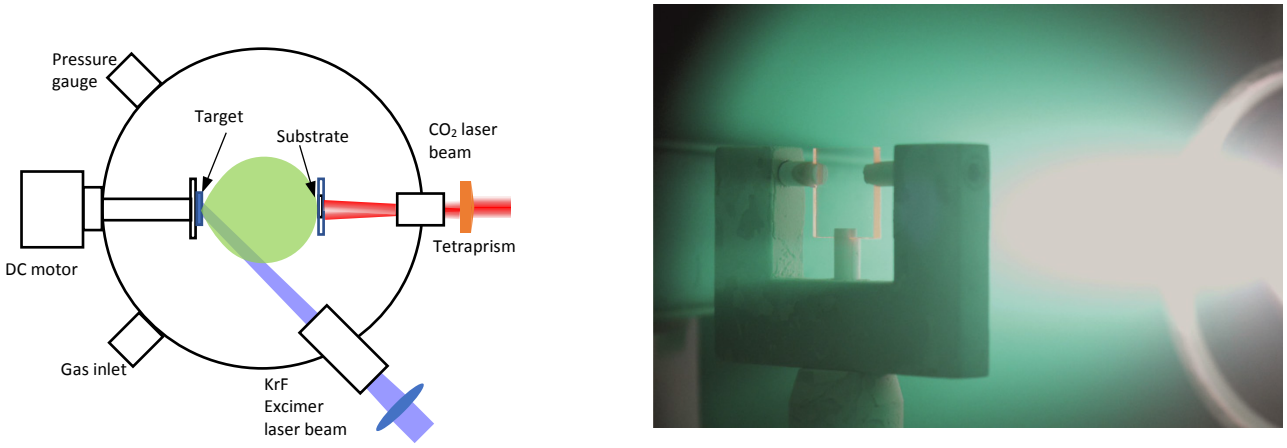

Fig 1. Schematic (left) and photograph of the PLD setup (right).

A KrF excimer laser (Coherent - COMPexPRO) was used in the growth of the waveguides described herein. Operating at a repetition rate of 100 Hz, with fluence levels of ~1.6 Jcm^{-2}, we achieve film growth-rates of up to ~25 μm/hour. The 1-mm thick × 1cm^2 YAG substrate is heated from behind by a homogenized CO_2 laser beam with ~11 W of incident power. No direct temperature measurement within the chamber is employed, as the repeatability based on incident power has been sufficient. Three separate targets with different erbium-dopant concentrations (1, 2, and 4 at.%) were used to fabricate the active YGG waveguides. Growth runs of nominally 1 hour were performed for the samples discussed herein.

A major challenge for PLD is the unwanted incorporation of particulates in the growing film. In the simplified schematic of Fig.1 it is clear that the incident UV laser beam is fixed at a unique angle. In our previous Er:YGG work [5] we employed a target-motion scheme that provided an epitrochoidal path across the surface, sweeping out a broad ablation path after many iterations of the target movement. At the same time the system maintains a static point of incidence so that the plume is originating from the same place. Although a large area of the target was utilized by this approach, every incident pulse originated from a unique angle with respect to the surface normal, which we term uni-directional ablation. We identified that the target surface was being modified through Laser Induced Periodic Surface Structuring (LIPSS), and these cone-like features would evolve with repeated ablation leading to "loose" particles on the target surface. Particulates are potentially created from the tips of the conical features during the explosive ablation process, which could then be transferred to the substrate [9]. With the motivation to improve the film quality a new scheme was implemented in the way the target is moved, such that on average, the incident ablation laser beam would appear to come from two equal and opposite directions [10], which we term bi-directional ablation. In this way the LIPSS of the target is frustrated and fewer particulates formed that could subsequently be transferred to the substrate and incorporated in the growing film.

2.2 Channel waveguide fabrication

Ridge waveguides were fabricated on the PLD-grown Er:YGG films by ultra-precision dicing, utilizing ductile mode machining [11, 12]. Dicing saws are often used to separate dies from wafers in the semiconductor industry. Typically cutting speeds are high for productivity and dies are often machined in the brittle mode of machining where large side wall surface roughness and micron-scale topside chipping is prevalent. In this work we optimized the dicing machining parameters by following a similar process discussed in pervious works [11, 12]. For this garnet material we used a Disco

DAD3430 dicing saw and a nickel bonded blade (Z09, Disco) with a small grit size (SD5000). A 40-µm depth of cut was used to remove the material in a single pass, at a feed rate of 20 nm/rev, an order of magnitude slower than the feed rate used to machine flame-hydrolysis-deposited silica [12]. Reverse osmosis water was used throughout as the coolant, at a rate of ~3 L/min, maintained at the lab temperature (21 ºC) to reduce temperature differentials whilst processing. Waveguides and facets were cut with the same parameters, with the waveguides parallel (and facets perpendicular) to the side edges of the substrate. Surface topology of the prepared facets was measured using a white light interferometer (ZeScope, Zemetrics) on five samples, in an 11 µm by 11 µm area and using a 100x magnification setting, roughness parameters were calculated after applying polynomial levelling.

2.3 Spectroscopic characterization

To characterize the erbium spectroscopic properties we first measured the fluorescence from the top-face (perpendicular to the waveguide) of the Er:YGG film when excited with a suitable pump laser through one facet of the waveguide. The emission was collected with a multimode-fiber patch cable (0.275NA, 62.5 µm core fiber) held in close proximity to the incident facet of the excited film, as shown in Fig. 2. An optical spectrum analyzer (OSA) (Ando AQ6317B) was used to record the emission spectra from the $^4I_{13/2}$ excited state. A very similar setup was used to determine the Er^{3+} lifetime, with the same pump beam focusing arrangement but with a pump filter between the patch fiber and transimpedance-amplified InGaAs photodiode (Thorlabs PDA10CS-EC). Measurements of the composition of the respective films were made with a Zeiss EVO LS25 scanning electron microscope (SEM) with an integrated Oxford Instruments INCAx-act X-ray detector for energy-dispersive X-ray analysis (EDX).

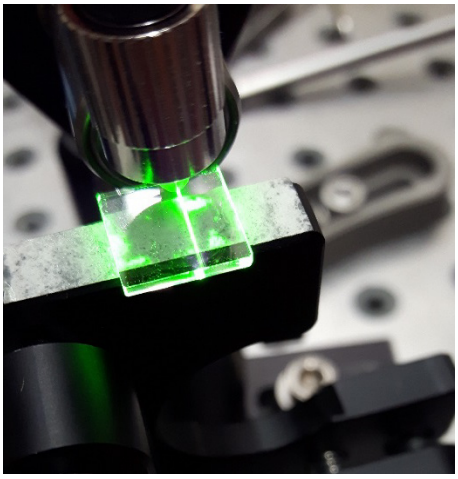

Fig 2. Photograph of the spectroscopic-measurement setup.

2.4 Waveguide characterization

Waveguide mode properties were investigated by measuring the beam profile (NanoScan 2S Ge – Ophir) at the position of the front facet of the waveguide, then comparing it to the image of the mode profile at the rear facet. Measurements were made when launching into the both ends of the waveguide, allowing us to determine which end would have the best coupling efficiency.

Gain measurements were undertaken by using a modulated pump (20 ms pulses at 10 Hz) and CW probe technique. Firstly the setup begins with wavelength multiplexing a 1480 nm Fiber Bragg Grating (FBG)-locked diode-laser pump with a narrow-linewidth seed source, the latter either a tunable diode-laser in the C- or L-band, or a DFB diode-laser at 1651 nm. These pump and seed lasers, coupled into one single-mode fiber, were free-space coupled to co-propagate in the waveguide under test, using an appropriate telescope magnification to optimize the launch efficiency. After the waveguide the transmitted light was collimated and reflected off a diffraction grating, spatially separating the pump and seed wavelengths after a focusing lens. The change in power of the seed was then monitored as a function of the pump power. A schematic of the setup is shown in Fig. 3.

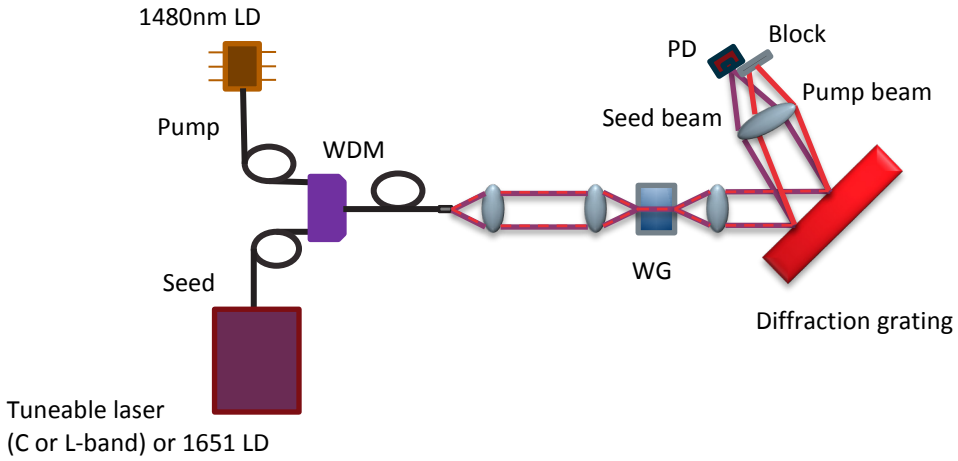

Fig 3. Schematic for the gain-measurements setup, with pump and seed lasers coupled by a wavelength division multiplexer (WDM), the output of which is launched into the waveguide (WG) and amplification measured at the photodiode (PD).

3. RESULTS

3.1 Bi-directional PLD

Dark-field (DF) microscopic images of the top surface of the fabricated films gives the simplest and most direct measure of defects, which we assume are primarily associated with particulates. From these images we are able to determine the area within the image that is above an intensity threshold value, corresponding to light reflecting back toward the sensor. For a perfect interface the image would be completely black. To compare respective films, the same illumination settings are employed and a threshold set to 10% of the peak pixel-intensity. Taking the ratio of the number of pixels with an intensity value above the threshold to the total number of pixels, provided a relative measure of the film quality. The closer this value of the "percentage covered area" is to zero the less the number of scattering centers there are. The DF insert in Fig 4(a) shows an example of a film with 3.25% defects, while in Fig.4(b) there are only 0.27%, corresponding to uni-and bi-directional ablation respectively. Histograms of the percentage of the area covered in a sample's DF image show that samples grown with uni-directional ablation, the mean value is (1.0 ± 0.22) % based upon 28 samples. While for bi-directional ablation the defects reduced by almost an order of magnitude to (0.17 ± 0.03) %, based upon 19 samples.

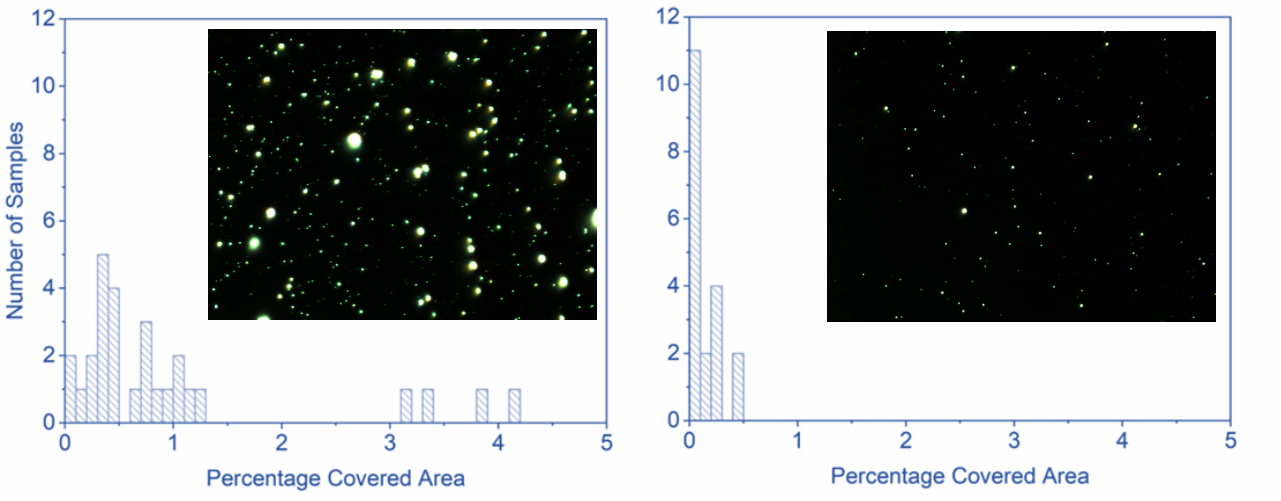

(a) (b)

Fig 4. Dark field statistical analysis for (a) uni-directional ablation vs (b) bi-directional ablation, with DF images corresponding to exemplar films (with an inset image size of 94 μm x 70 μm). DF image (a) has a 3.25% coverage with scattering defects, while in (b) it is 0.27%.

It should be highlighted, that there are many other factors influencing the defect count in PLD grown films, however the health of the target clearly has a very strong effect. Optimization of the process parameters should lead to further improvements in film quality.

3.2 Channel waveguides

Ridges of the PLD-grown Er:YGG films on YAG were made with varying widths from ~13-28 µm. The measured average (S_a) and RMS (S_q) surface roughness of the machined surfaces on the perpendicular facets, were equal to 3.8 ± 1.9 nm and 5.1 ± 2.5 nm, respectively. Microscope images of the dicing-blade-polished end facets are shown in Fig. 5, with the PLD ridge supported on a YAG substrate pillar, after the side material was removed. A nearly perfectly perpendicular side-wall was obtained on one side, as shown in Fig. 5(b), with a small inclination of the other.

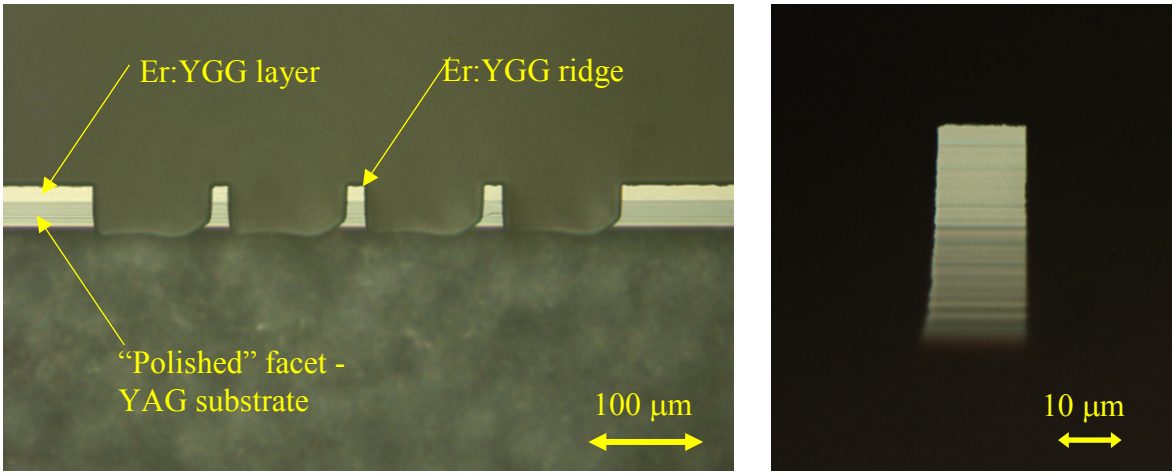

(a) (b)

Fig. 5: (a) Microscope image of the end facets of three adjacent Er:YGG ridge channel waveguides. (b) 100x magnification image of just one ridge.

3.3 PLD-grown Er:YGG spectroscopy

Taking a measurement of the fluorescence lifetime, as shown in Fig. 6(a), along with the spectral power density, then applying the Füchtbauer-Ladenburg equation, we obtain the emission cross section, assuming a radiative lifetime of 5.9 ms [13]. The ratio of the measured lifetime and the radiative lifetime gives the quantum efficiency, η_{QE} ~92%, for the $^4I_{13/2}$ level in this material, noting that it may not only be multi-phonon non-radiative transfer to the ground state, but also energy migration to defects and impurities in the film that influence this value. Utilizing the Stark level assignments for Er:YGG [13], McCumber theory provides the absorption cross section, as shown in Fig 6(b). The shape and magnitude of the calculated cross sections are in very good agreement with that observed in bulk crystals made via traditional techniques [2]. As demonstrated in Fig. 6(b) there are emission peaks corresponding to the wavelengths of interest around 1572 nm and 1651 nm. Similar spectra were obtained for each of the three erbium doping levels trialed. Confirmation of the absorption cross section was obtained for wavelengths below 1500 nm by proximity coupling a single-mode optical fiber to the channel waveguide facet, into which the light from a halogen lamp had been launched. The relative transmission of the white light through the waveguide provided a measure of the absorption coefficient offset by the waveguide propagation and coupling losses. From the absorption coefficient an ion density was determined for the respective doping levels as shown in Table 1. This is compared to the value determined through EDX measurement and found to be smaller in each case, although in reasonable agreement considering the uncertainties of both techniques. It is worth highlighting that some Er^{3+} ions may not be in the correct crystallographic site, i.e. substituting for gadolinium, rather than yttrium [13].

Table 1. Comparison of erbium ion density for the respective targeted doping levels (1, 2, and 4at.%) Er^{3+}

Doping concentration for the tested Er:YGG films		
Sample #	Ion density (absorption) ($\times 10^{20}$ cm^{-3})	Ion density (EDX) ($\times 10^{20}$ cm^{-3})
1 (1 at.%)	0.74 +/- 0.15	1.0 +/- 0.1
2 (2 at.%)	1.82 +/- 0.18	1.9 +/- 0.2
3 (4 at.%)	4.60 +/- 0.46	4.9 +/- 0.5

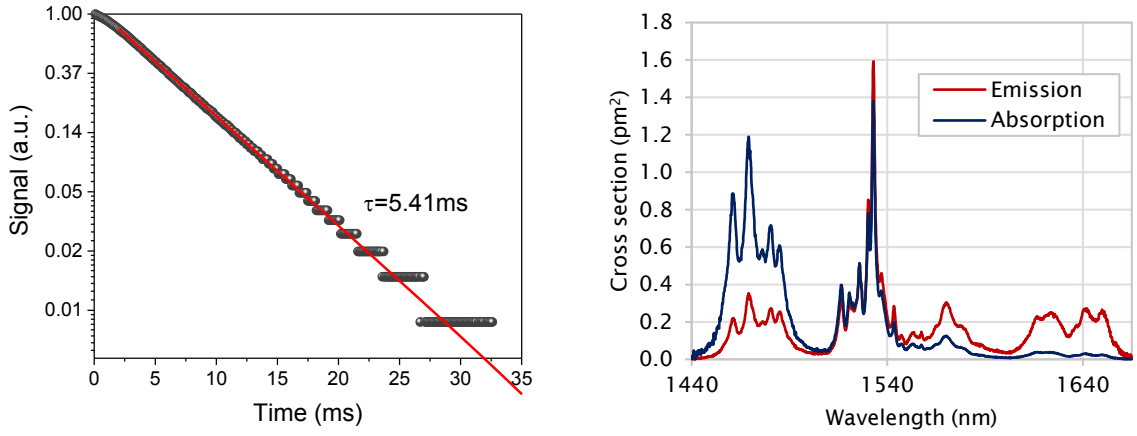

(a) (b)

Fig. 6: (a) Fluorescence lifetime measurement for sample # 3. (b) Calculated emission and absorption cross sections for transitions between $^4I_{13/2} \leftrightarrow {}^4I_{15/2}$ in PLD-grown Er:YGG crystal films.

3.4 Waveguide characteristics and amplifier performance

The beam profile of the imaged output-fiber facet of the WDM, at the input plane of the channel waveguide, is shown in Fig. 7(a). Fig. 7(b-c) are the measured mode profiles exiting an exemplar channel, with the sample firstly oriented one way (b), then reversed (c). The different profiles show that there are asymmetries in the shape of the ridge, which is mainly attributed to slight thickness differences at either end of the substrate and the minor inclination of one side wall.

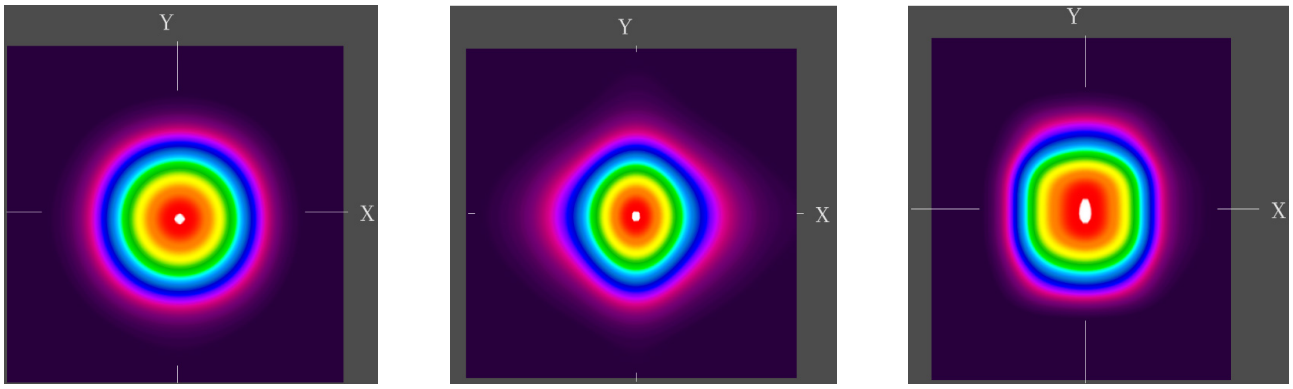

(a) (b) (c)

Fig. 7: (a) Beam profile images of (a) input beam ($\phi_{D4\sigma}$=10.4 μm), (b) mode profile at one end facet of the Er:YGG ridge channel waveguide on sample #2 (D4σ_x=10.6 μm, D4σ_y=10.4 μm), and (c) at the other end of an (D4σ_x=10.8 μm, D4σ_y=12.4 μm)

When measuring the achievable gain for individual channels, the facet used was that for which the supported mode had the best mode overlap with the input beam. A typical temporal response for the CW 1651 nm seed, monitored during the pumping pulse, is shown in Fig. 8(a), corresponding to peak incident pumping powers ranging from 39 mW to 353 mW. These power levels correspond to an incident intensity of I_p = 46 kWcm^{-2} to 416 kWcm^{-2}, well in excess of the pump saturation intensity at 1480 nm equal to I_p^{Sat} = 2.7 kWcm^{-2}. As shown in Fig. 8(a) for 3.5 mW (I_s = 4.1 kWcm^{-2}) of 1651 nm incident seed power (intensity), 2.37 mW is transmitted indicating a combined coupling, Fresnel, propagation, and absorption loss of -1.7 dB, associated with the launch into the channel. Extracting the Fresnel losses associated with both facets, -0.85 dB, provides a base loss to overcome for achieving internal gain. For the ~1 cm-long sample #2 waveguide, nominally 2at.% Er:YGG, we observed maximum internal gains of 3.46 dB, 0.54 dB, and 0.53 dB at the respective wavelengths of 1533 nm, 1572 nm, and 1651 nm.

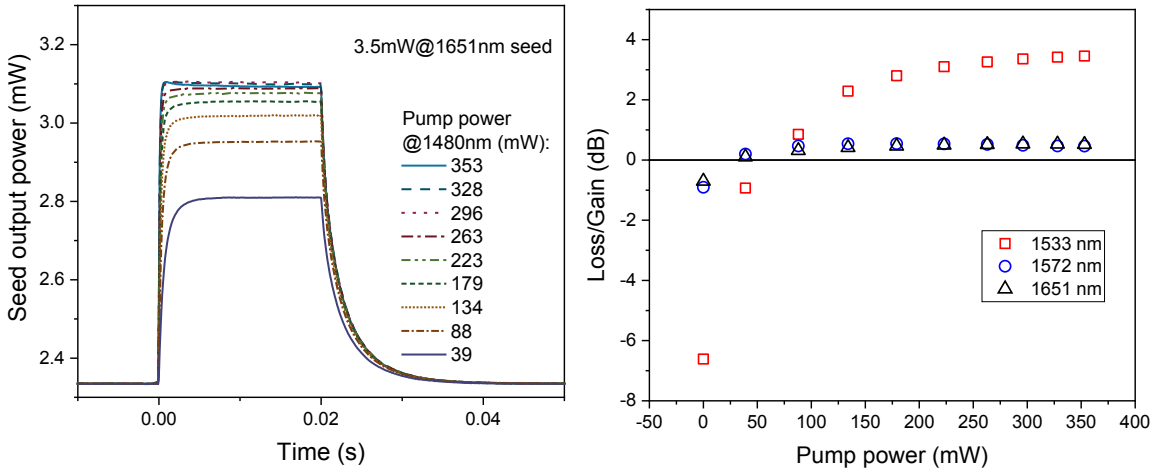

(a) (b)

Fig. 8: (a) Temporal response for the transmitted 1651 nm seed power exiting the channel (including losses associated with Fresnel reflections), for the channel waveguide in sample #2, with modal distributions presented in Fig. 7. (b) Internal loss/gain measured for 1533 nm, 1572 nm, and 1651 nm, as a function of incident pump power in the same channel.

4. DISCUSSION

With the bi-directional PLD protocol, an order of magnitude lower defect density in the grown crystal films was obtained, when compared with the classic uni-directional ablation method. This manifests itself in reduced propagation losses as realized in the channeled samples detailed herein, some better than -0.3 dB/cm, compared with similar planar films reported in [5] of -0.8 dB/cm. Channels were fabricated with widths ranging from ~13 μm to ~19 μm, with ductile-dicing leading to optical quality surface roughness and the low propagation losses along the waveguide. Slight asymmetry in the ridge profile can be improved through optimization of the dicing process and uniformity of the grown films. With such improvements it will be possible, for example, to improve the mode-matching to single-mode fiber, which would enable fiber pig-tailed devices to be made.

Three different doping levels were tested in this work, corresponding to 1, 2, and 4 at.% Er^{3+} in the targets. From measurement of the rare-earth density in the crystal layers it appears that on average only ~80% of these active ions are integrated into the grown films. The spectroscopy of the films is well matched with that expected for Er:YGG and provides fortuitous gain peaks at the key wavelengths of interest for atmospheric CO_2 and CH_4 monitoring. For the three samples detailed here record gain-per-cm levels have been achieved for the respective wavelengths in erbium-only doped waveguide amplifiers. A summary of the measured maximum internal gains for each of the samples is given in Table 2.

Table 2. Comparison of internal gain for the respective samples

Sample #	**Channel dimensions x × y (μm)***	**Coupling, absorption, and propagation loss** dB @1651nm**	**Maximum internal gain, dB**		
			1533nm	**1572nm**	**1651nm**
1	25 x 18	-0.27	1.57	0.45	0.35
2	14 x 14	-0.9	3.46	0.54	0.53
3	16 x 19	-1.2	-3.31	0.41	0.44

* x – width axis, y – height or film thickness; ** Fresnel losses removed

At higher pump powers notable parasitic effects were observed to reduce the achievable gain, just noticeable in Fig. 8(a), which is assumed to be due to excited state energy transfer pathways and thermal effects through mode coupling in these multi-mode channel waveguides. These effects were more pronounced in the higher concentration waveguides, as may be expected with increased heat loading density and energy transfer coefficients due to the tighter packing of the Er^{3+} ions.

5. CONCLUSIONS

We have, for the first time, fabricated and tested Er:YGG channel waveguides made by ultra-precision dicing, in the ductile regime, of ridges in thick-films grown by pulsed laser deposition. Material and waveguide properties were evaluated and show comparable spectroscopic parameters to that obtained from Czochralski grown material, and the lowest waveguide losses yet obtained for equivalent waveguides. These properties have enabled record gain-levels to be achieved in our cm-long channel waveguide amplifiers, at each of the three key wavelengths tested. It is expected that with further optimization of the film quality, PLD-grown Er:YGG will be a promising candidate for waveguide amplifiers in the spectral regions that cover both CO_2 and CH_4 absorption bands.

REFERENCES

[1] Abdalati, W., Gail, W. B., Busalacchi, A. J. *et al.*, [Thriving on Our Changing Planet: A Decadal Strategy for Earth Observation from Space] The National Academies Press, Washington, DC(2017).

[2] Stange, H., Petermann, K., Huber, G., and Duczynski, E. W., "Continuous wave 1.6-micron laser action in Er-doped garnets at room-temperature," Applied Physics B-Photophysics and Laser Chemistry, 49(3), 269-273 (1989).

[3] Kudryashov, I., and Kotelnikov, E., "Tunable Q-switched Solid State Laser for Methane Detection," Proceedings of SPIE. 10082.

[4] Yu, A. W., Betin, A., Krainak, M. A. *et al.*, "Highly efficient Yb:YAG master oscillator power amplifier laser transmitter for lidar applications," 2012 Conference on Lasers and Electro-Optics (CLEO), 2 pp.-2 pp. (2012).

[5] Mackenzie, J. I., Grant-Jacob, J. A., Beecher, S. *et al.*, "Er:YGG Planar Waveguides Grown by Pulsed Laser Deposition for LIDAR Applications," Proceedings of SPIE. 10082.

[6] Grant-Jacob, J. A., Beecher, S. J., Parsonage, T. L. *et al.*, "An 11.5 W Yb:YAG planar waveguide laser fabricated via pulsed laser deposition," Optical Materials Express, 6(1), 91-96 (2016).

[7] Beecher, S. J., Grant-Jacob, J. A., Hua, P. *et al.*, "Ytterbium-doped-garnet crystal waveguide lasers grown by pulsed laser deposition," Optical Materials Express, 7(5), 1628-1633 (2017).

[8] Parsonage, T. L., Choudhary, A., Beecher, S. J. *et al.*, [Comparative study of rare-earth doped sesquioxides grown by pulsed laser deposition and their performance as planar waveguide lasers] OSA, Munich, Germany(2015).

[9] Grant-Jacob, J. A., Prentice, J. J., Beecher, S. J. *et al.*, "Particulate reduction in ternary-compound film growth via pulsed laser deposition from segmented binary-targets," Materials Research Express, 5(3), (2018).

[10] Prentice, J. J., Grant-Jacob, J. A., Kurilchik, S. V., Mackenzie, J. I., and Eason, R. W., "Particulate reduction in PLD-grown crystalline films via bi-directional target irradiation," Applied Physics a-Materials Science & Processing, 125(2), (2019).

[11] Carpenter, L. G., Berry, S. A., and Gawith, C. B. E., "Ductile dicing of LiNbO3 ridge waveguide facets to achieve 0.29 nm surface roughness in single process step," Electronics Letters, 53(25), 1672-1673 (2017).

[12] Carpenter, L. G., Rogers, H. L., Cooper, P. A. *et al.*, "Low optical-loss facet preparation for silica-on-silicon photonics using the ductile dicing regime," Journal of Physics D-Applied Physics, 46(47), 8 (2013).

[13] Ashurov, M. K., Voronko, Y. K., Osiko, V. V., Sobol, A. A., and Timoshechkin, M. I., "Spectroscopic study of stoichiometry deviation in crystals with garnet structure," Physica Status Solidi a-Applied Research, 42(1), 101-110 (1977).